


Sensor-based localization of epidemic sources on human mobility networks

Jun Li¹^{□a}, Juliane Manitz¹^{□b}, Enrico Bertuzzo², Eric D. Kolaczyk^{1*}

1 Department of Mathematics & Statistics, Boston University, Boston, MA, USA

2 Dipartimento di Scienze Ambientali, Informatica e Statistica, University of Venice Cà Foscari, Italy

 These authors contributed equally to this work.

□a Current Address: Google, Mountain View, CA, USA

□b Current Address: EMD Serono, Billerica, MA, USA

* kolaczyk@bu.edu

Abstract

We investigate the source detection problem in epidemiology, which is one of the most important issues for control of epidemics. Mathematically, we reformulate the problem as one of identifying the relevant component in a multivariate Gaussian mixture model. Focusing on the study of cholera and diseases with similar modes of transmission, we calibrate the parameters of our mixture model using human mobility networks within a stochastic, spatially explicit epidemiological model for waterborne disease. Furthermore, we adopt a Bayesian perspective, so that prior information on source location can be incorporated (e.g., reflecting the impact of local conditions). Posterior-based inference is performed, which permits estimates in the form of either individual locations or regions. Importantly, our estimator only requires first-arrival times of the epidemic by putative observers, typically located only at a small proportion of nodes. The proposed method is demonstrated within the context of the 2000-2002 cholera outbreak in the KwaZulu-Natal province of South Africa.

Author summary

Tracking the source of an epidemic outbreak is of crucial importance as it allows for identification of communities where control efforts should be focused for both short and long-term management and control of the disease. However, such identification is often problematic, time-consuming, and data-intensive. Recently network-based analysis approaches have been established for source detection to account for complex modern spreading, driven substantially by human mobility. Here we develop a probabilistic framework for waterborne disease, that allows investigators to infer the community or the region sparking an outbreak based on a sparse surveillance network. The framework can integrate prior information on the likelihood of a community being the source, for instance as a function of population size or hygiene conditions. Furthermore, we assign an accuracy measure to the resulting source estimate, which is crucial for its practical usability. We test the method in the context of the 2000-2002 cholera outbreak in the KwaZulu-Natal province with promising results. Moreover, we outline a series of guidelines in terms of data needs and preliminary operations to implement the proposed framework in practice.

Introduction

One of the most important factors in epidemic control is to trace the source or origin of an epidemic [1,2]. This problem is sometimes called ‘source localization’ (and can in fact involve multiple sources). Ideally, one would like to locate the source based on data capturing the entire history of the epidemic, including times of infection / recovery of individuals as well as information on contact between individuals and of individuals with infective aspects of the environment (e.g., water sources). However, epidemic history is complex and high-dimensional, and almost invariably the data are incomplete – often substantially so [3,4].

Over the past 5-10 years, researchers have found it useful to reformulate the localization problem as that of estimating a source node(s) on a complex network. There have been a large number of contributions in this area to date. A recent and comprehensive review has been conducted by [5]. Many approaches use network-distance-based measures of centrality to identify the source node in a complex network, such as rumor centrality [6,7] or Jordan centrality [8,9]. A related idea is that of effective distance-based source detection [10,11]. However, typically these methods assume network-wide observation of the infection status of nodes at either a single time point or a handful of such snapshots, which is generally unrealistic for large networks – particularly in the context of human disease. Alternatively, sensor-based methods are designed to instead locate a source based on arrival-time information of infection from only a subset of observer nodes (e.g., [12,13,29]).

Despite the development in this area, there is still substantial room for improvement [5]. In general, methods proposed to date frequently fail to assimilate the often-abundant information that can be gained through epidemic modeling, as well as additional prior information. In addition, they typically do not provide measures of uncertainty quantification. Both of these aspects are especially important in the context of human disease, where policy providers and decision makers are often data-poor and yet required to make concrete decisions that have pronounced impact on society. In this paper, focusing on the illustrative example of cholera epidemics, we propose a method of source detection that integrates (i) a sensor-based approach, with (ii) a stochastic differential equation model for water-borne disease. In turn, we adopt a Bayesian framework, thus allowing for uncertainty quantification and the formal use of prior information.

A key component of our approach is the incorporation of human mobility networks. Human mobility is one of the main drivers for the spreading of infectious diseases. Understanding, predicting and possibly controlling the propagation of an epidemic in a population cannot prescind from the analysis of the underlying human mobility patterns. Historically, network-based research incorporating human mobility has focused on infectious diseases transmitted through direct contact between individuals e.g. [15–18]. However, the role of human mobility in the spreading of waterborne diseases (where transmission is mediated by water) has also recently attracted increasing attention e.g. [19,21–23]. Indeed, a susceptible individual can be exposed to contaminated water while travelling or commuting and seed the infection in the resident community once back. On the other hand, asymptomatic infected individuals (who potentially shed pathogens but whose movement is not impaired by the disease symptoms) can spread pathogens while moving among different human communities. These two mechanisms highlight the critical role of human mobility as a notion extending beyond direct contact.

In this paper, we recast the source detection problem as one of identifying the relevant mixture component in a multivariate Gaussian mixture model from [12]. Human mobility within the stochastic, spatially-explicit epidemiological model of [23] is used to calibrate the parameters. Our estimator requires only first-arrival times of the

epidemic at a small proportion of nodes, termed sensors or observers. Adopting a Bayesian perspective opens the possibility to seamlessly integrate available nontrivial prior knowledge from previously observed spreading patterns or other data sources. Moreover, we are able to quantify uncertainty in the resulting estimators. Specifically, our approach provides (a) statistically well-defined region(s) of nodes that are likely to be the spreading origin of the observed process, accompanied by a corresponding posterior probability.

We develop and apply our method in the context of the 2000–2002 cholera outbreak in the KwaZulu-Natal province, South Africa. In particular, our integrative, Bayesian approach demonstrates significant improvement in this context over the use of a generic sensor-based source detection approach alone [12].

To better place our contributions in context, we note the following points in comparison to related work in the literature. First, while there are a number of network-based methods of epidemic source detection that are not generic and that incorporate some knowledge of disease epidemiology (e.g., [24–26]), this is the first article to integrate cholera-specific transmission models in network-based source detection. Second, while human mobility networks have been used previously in network-based epidemic source detection (e.g., [27], who also use a gravity model similar to ours), this is the first article to integrate the role of human mobility in the complex spreading of waterborne diseases. Finally, while a number of Bayesian approaches have been suggested or developed in epidemic source detection (e.g., [24, 25, 28]), to the best of our knowledge none of these have developed an informed prior probability distribution. In addition, while our use generic networks for the underlying spreading pattern is less common in the literature (in contrast to assuming a tree-like structure), there is indeed precedent (e.g., [26, 29]).

Code implementing our proposed method has been integrated into the *NetOrigin* package in R.

Results

Sensor-based source localization: overview of proposed method

We assume a network $G = (V, E)$ to be given that is composed of a set of nodes $v \in V$ that are inter-connected by links $(u, v) \in E$. Furthermore, there is a spreading process on this network, which originates in source node $s^* \in V$. For pre-defined sensors at a small fraction of nodes, $O = \{o_k\}_{k=1}^K$, $K \leq |V|$, we observe the first-arrival times of the spreading process, i.e. $\mathbf{t} = (t_1, \dots, t_K)^\top$. In the epidemiological context motivating our work, the set of nodes $v \in V$ are human communities, and the first-arrival times are the time points at which a given level of disease incidence is attained in observed communities. Our aim is to develop a good estimator for the source s^* and to quantify the uncertainty in that estimator.

Conditional on the underlying spreading process and a given source s^* , the first-arrival times \mathbf{t} are assumed to follow a K -dimensional multivariate Gaussian distribution. The *a priori* chance that a given node s is the epidemic source is modeled according to a prior distribution $\boldsymbol{\pi} = (\pi_1, \dots, \pi_N)^\top$ over network nodes $v \in V$ with $\sum_{v=1}^N \pi_v = 1$, where $N = |V|$ is the total number of nodes. Through this prior we incorporate subjective beliefs or other sources of information about the origin of the spreading process. Statistical inference on source location is then based on the corresponding posterior, with the most probable source determined as

$$\hat{s} = \arg \max_{s \in V} P(S = s | \mathbf{t}) , \quad (1)$$

and the most probable region, by

$$\hat{C} = \{s : P(s|\mathbf{T} = \mathbf{t}) > \tau_\alpha\}, \text{ so that } \sum_{s \in \hat{C}} P(s|\mathbf{T} = \mathbf{t}) \geq 1 - \alpha, \quad (2)$$

where here $\alpha \in (0, 1)$ is pre-specified and $\tau_\alpha \in (0, 1)$ is the largest such threshold for which the conditions in (2) hold.

The underlying spreading process is modeled using a set of stochastic differential equations for the spread of water-borne disease, consisting of three main elements. First, fundamentally, our model is a version of the well-known susceptible-infected-removed (SIR) model, but expanded to differentiate rates of death cross each class of individuals as well as to include components for both symptomatic and asymptomatic infection. Most of the rate parameters are simple constants to be set by the user (e.g., using historical data, public records, etc.). However, second, the rates of (a)symptomatic infection are modeled proportional to a ‘force of infection’ term which, for a given location, summarizes the aggregate contribution of bacterial concentration at neighboring locations and the extent of human mobility from the latter to the former location. Finally, third, the bacterial concentration at each location is modeled using a linear differential equation that includes a term reflecting the number of infected individuals and the volume of the local water reservoir.

Human mobility is represented through the network G , which is taken to be directed and weighted. Here nodes correspond to communities and weights on links between nodes reflect the probability of movement by individuals from one node to another. In our applications, these probabilities are calculated using a simple gravity model, combining information on the size of communities and the distance between them.

Our overall approach to sensor-based source localization combines a Bayesian extension of the method in [12] with the human mobility portion of the spreading model in [21]. By construction, the source localization problem in our setting effectively reduces to that of identifying through the posterior distribution the relevant component in a multivariate Gaussian mixture model. The necessary parameters for the individual Gaussian components, i.e., the means and covariances of the first-arrival times observed at sensors $1, \dots, K$, are calibrated using a combination of stochastic simulation from our spreading model and statistical smoothing of the corresponding output. These simulations in turn are run using various rate parameters whose values are retrieved through literature review. Additional details regarding modeling and implementation can be found in Methods.

Analysis of the 2000–2002 South African cholera outbreak

We applied our source estimation approach to data from the 2000–2002 cholera outbreak in the KwaZulu-Natal province, South Africa. The outbreak lasted for two years, starting in August of 2000, and ultimately involved about 140,000 recorded cases in two major waves in the respective summers [30]. Figure 1 shows the epidemic curve. We can see the peak of the first wave is much higher than the peak of the second wave.

Figures 2 and 3 show a spatial representation of some of the data and results relevant to our model. These data have already been described in detail in [21]. In the figures are shown the spatial locations of $N = 851$ communities in the KwaZulu-Natal province, indicated by dots for which the area scales with population size. In turn, each community corresponds to a node in our human mobility network G . A visualization of this network is also provided, as an overlay. In order to improve interpretability, only the three most frequented outbound links are shown (typically corresponding to roughly 10% of the outward mobility from a node). Among those links, we split them into 2 sets: the links with top 10% weights and those with bottom 90% weights. For the first set,

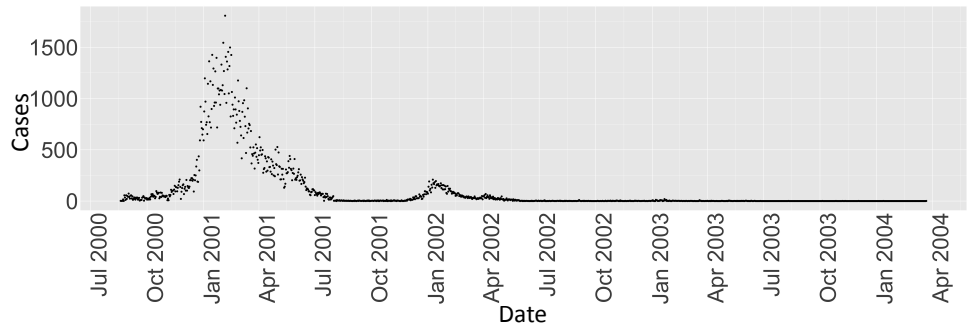


Fig 1. Number of cases per day in the 2000-2002 KwaZulu-Natal cholera epidemic.

we kept their weights unchanged; for the second set, we decreased their weights to 10% of their original value. That is sufficient to illustrate several characteristics of the network. In particular, we note the local, grid-like connectivity of much of the network, which is then complemented by a handful of nodes with substantially higher and more global connectivity. The network visualization suggests small-world behavior, which can be confirmed through computational methods applied to the underlying human mobility network (see the Supplemental Text (S1 File)). The more highly connected nodes with global connectivity correspond roughly to (i) Durban, the largest city in KwaZulu-Natal, and other cities in the Greater Durban Municipality (e.g., Inanda); (ii) Pietermaritzburg, the capital and second-largest city in KwaZulu-Natal, situated 80 km inland from Durban; and (iii) Newcastle, the third largest city, located near the northwest edge of the province.

Also represented in Figures 2 and 3 is a local version of the basic reproduction number, R_0 , for each community, through appropriate shading of the nodes. In epidemiology, the basic reproduction number of an infection can be thought of as the number of cases to derive from one infected case on average over the course of its infectious period, in an otherwise uninfected population [2]. In a well-mixed population, when $R_0 < 1$, the infection will die out in the long run. On the contrary, if $R_0 > 1$, the infection will spread. In the case of multiple interconnected local populations, the concept of basic reproduction number has been generalized by [31, 32]. Here, a local version of the reproduction number has been computed for each node, following the approach of [21], which combines information on community size with models for contamination and exposure rates that incorporate access to (in)adequate toilet facilities and to water, respectively. See Methods for additional details.

For each wave, nine nodes with highest weighted degree (also called node strength) in the human mobility network were chosen, from among those nodes that were infected during a given wave, to serve the role of ‘observers’ (or sensor nodes) in our source detection algorithm. These represent roughly 1% of the total nodes in the underlying network for each wave. Selecting observer nodes based on degree is expected to improve detection accuracy. (We examine this assertion further in the synthetic experiments described later in this section.) We see that the two resulting sets of observer nodes are largely complementary in nature. The observer nodes for Wave 1, shown in Figure 2, are spread throughout much of the province, to the north and northwest of Durban / Pietermaritzburg and to the south and southeast of Newcastle. In contrast, the observer nodes for Wave 2, shown in Figure 3, are concentrated almost entirely between these two major metropolitan regions.

Now consider the results of our source detection methodology applied to these data. Shown in Figure 4 are the posterior probabilities for those ten nodes found to have the largest chance of being a source node, for each of Wave 1 and 2, under both a uniform prior on nodes and a prior proportional to the local R_0 . For each of the four

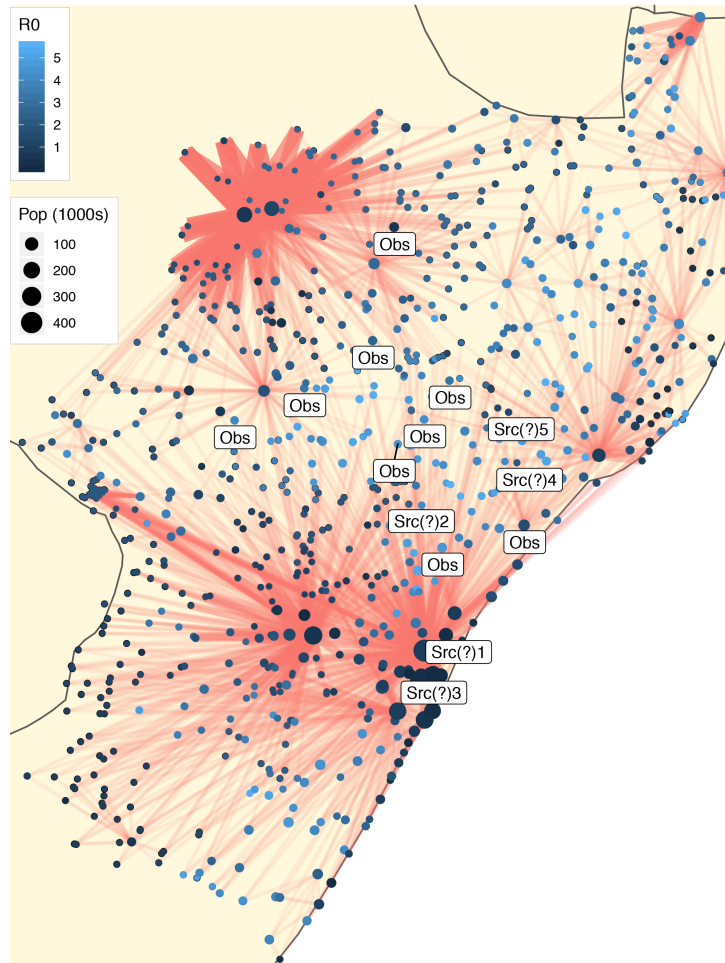


Fig 2. The human communities of the KwaZulu-Natal Province and their corresponding mobility network (showing only three most frequently outbound links), with nodes sized and colored to indicate population and R_0 , respectively. Labels indicate nine ‘observer’ nodes and top five putative sources for Wave 1 of the cholera epidemic, as identified by our proposed methodology (based on a uniform prior).

combinations of wave and prior, the corresponding ten nodes ended up representing a most probable posterior region of roughly 0.70 posterior mass. In comparing results for the two waves, there is clear evidence that the posterior in Wave 1 is substantially more concentrated on just one (R_0 prior) or two (uniform prior) nodes. On the other hand, while in Wave 2 there is some evidence of similar concentration under the uniform prior, with the R_0 prior there is comparatively less information in the posterior to differentiate the ten most probable nodes. Accordingly, we see that incorporating prior information in the form of the local reproduction numbers (which in turn reflect a combination of community size with contamination and exposure rates) has a substantive impact on the shape of the corresponding posterior distributions.

To understand the impact of these differences in posterior shape on the rankings of putative sources (and, hence, the potential impact on decisions of policy, resources, etc.), consider the plots in Figure 5. Overall, it would seem that the ranks are fairly stable, with seven and eight of those nodes ranked top-10 under the uniform prior still remaining in the top-10 under the R_0 prior, for Waves 1 and 2, respectively. However, there are important exceptions. For example, in Wave 1, there are four points whose

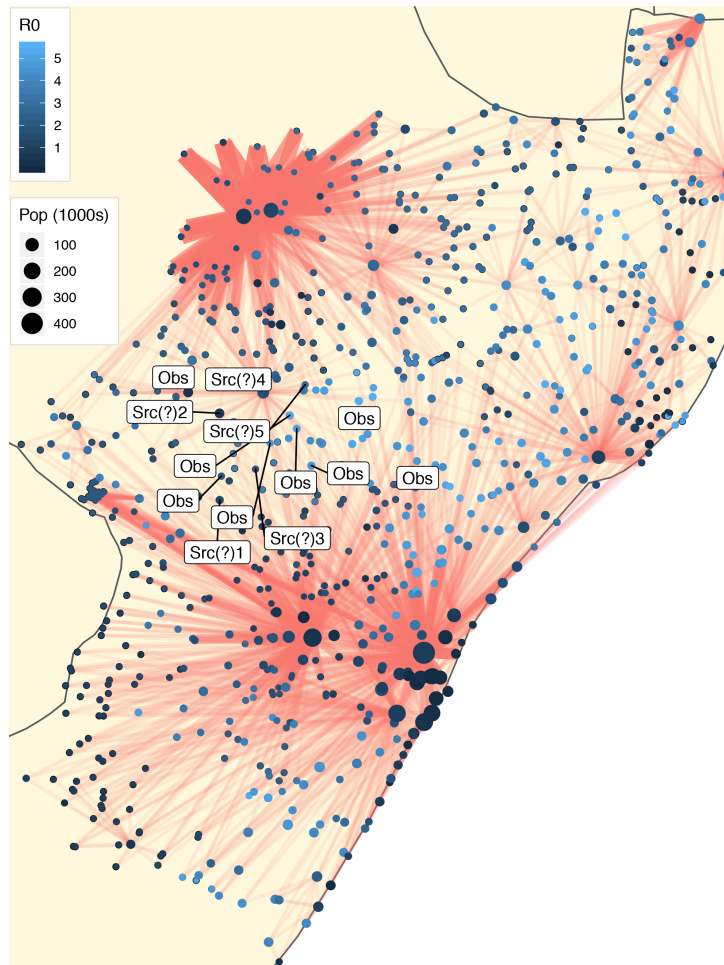


Fig 3. The same human communities mobility network as in Figure 2, but with observers and putative sources corresponding to analysis of Wave 2 of the cholera epidemic. (Note: The fourth putative source is also an observer node.)

initial rankings change considerably by including R_0 information (three of which drop well out of the top-10), all of which have very small R_0 (i.e., 0.21 or less). Interestingly, one of these four corresponds to the top-ranked node under the uniform prior, which nevertheless remains top-10 under the R_0 prior (i.e., ranked 7th), suggesting that the evidence in the data towards it being a source is particularly strong. On the other hand, another of these nodes drops from third to 16th.

Although there is no ground truth for these data, some conjectures can be made based on these results. As can be seen from the map in Figure 2, these two nodes (i.e., the first and third ranked putative sources under the uniform prior) are in fact geographically quite close together and located in the vicinity of Durban. They correspond roughly to Town Verulam and Westville, respectively. The first is located on the coast about 27 kilometers north of Durban, and the second, about 10 kilometers to the west of Durban. Both have comparatively large populations and low R_0 . In contrast, the node corresponding to an area called Eshane has a small population (~ 500) with a very large R_0 (7.18), and yet is ranked the second most likely source under either choice of prior. Eshane is about 45 kilometers east of Greytown, a town situated on the banks of a tributary of the Umvoti River in a fertile area that produces

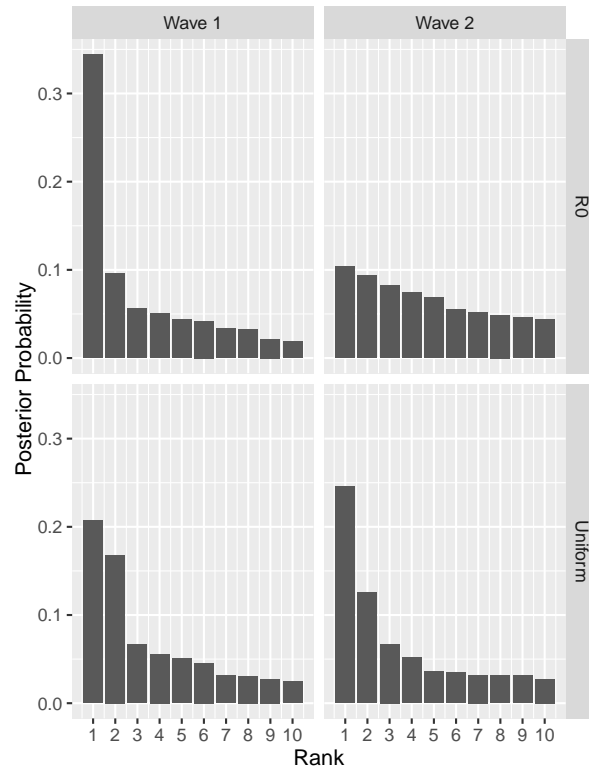


Fig 4. Ten largest posterior probabilities $P(S = s|t)$ (sorted by magnitude) for source detection during Waves 1 (left) and 2 (right) of the 2000–2002 cholera epidemic in KwaZulu-Natal, South Africa, under a uniform prior (bottom) and a prior proportional to local R_0 (top).

timber, and which sits at the nexus of multiple regional routes (i.e., R33, R74 and R622) which might help the waterborne disease, cholera, to spread. Examination of the epidemic time course for Wave 1 shows that the wave was first found to spread largely along the coast (see Supplemental Figure 6). Together, therefore, these observations suggest that the results of our analysis of Wave 1 can be interpreted as saying that either (i) the epidemic originated in the interior (near Eshane) and was brought to the coast, or (ii) it in fact originated on the coast (just outside of Durban).

In comparison, the results of our analysis for Wave 2 seem to tell a consistent story, whether under the uniform prior or the R_0 prior, in that the two most likely putative sources are the same for either choice of prior (albeit with their order switched) and are located fairly close together. As seen from the map in Figure 3, application of our methodology indicates that the epidemic source for this wave lies inland, in the more sparsely populated central region of the province between the two major metropolitan areas of Durban / Pietermaritzburg and Newcastle. Under the uniform prior, the most likely source is Ezakheni E, a town of moderate population size and somewhat elevated R_0 (i.e., 1.67). And about half as likely is the town of Estcourt, about 60 kilometers south, also of moderate (although smaller) population size but with substantially larger R_0 (i.e., 3.62). Alternatively, under the R_0 prior, these two nodes have nearly equal (and lower) posterior probability of being a source. Examination of the epidemic time course for Wave 2 shows that, while the earliest reported cases were to the north and northeast of the region surrounding these two nodes (i.e., near Newcastle), the bulk of the infections during this wave seemed to concentrate in this region (see Supplemental

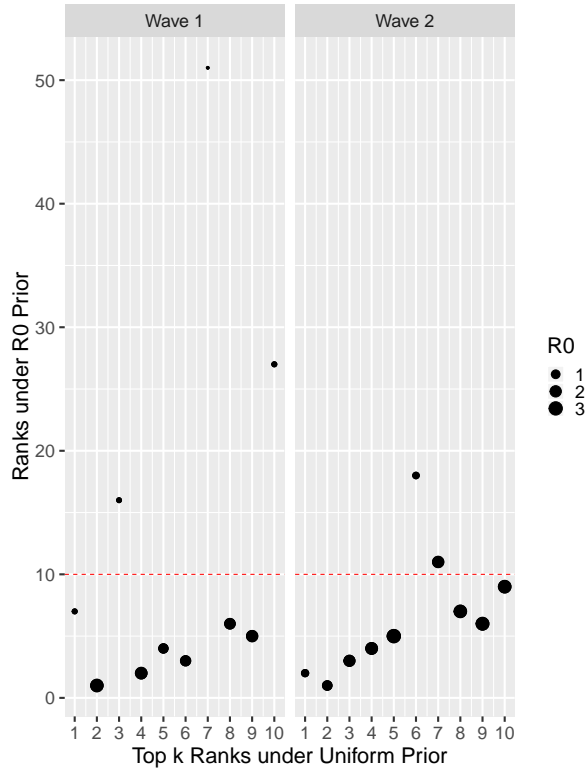


Fig 5. Visualization of the extent to which posterior-based ranking of the top ten putative source nodes, under the uniform prior (x-axis), change when using the R_0 prior instead (y-axis), for Waves 1 (left) and 2 (right). The size of each point in the scatterplots is in proportion to the R_0 value for the corresponding node.

Figure 7). Therefore, the results of our analysis suggest that this second wave most likely originated from this central region, between the two larger metropolitan areas, and spread outward from there, perhaps through the system of rivers flowing through the area (i.e., Ezakheni E and Estcourt lie close to the rivers Kliprivier and Boesmansrivier, respectively).

In the above analyses, a node was said to be infected once the prevalence (i.e. the number of infected individuals) first exceeds 0.1% of the population. Additional analysis shows that our results (i.e., the top-ten ranked nodes) remain robust when this choice of threshold is decreased to 0.09% and even 0.05%, but deteriorates at 0.01% (see Fig 14, in Supplemental Materials). At the same time, thresholds larger than 0.1%, even 0.2%, makes the inference procedure fail, since not all observers are infected. Formally, this failure could be avoided through appropriate adjustments to the underlying formulas and procedures (i.e., accounting for right-censoring in the data for these nodes), but one would still nevertheless expect a deterioration in performance.

Synthetic experiments

In order to gain some insight into the reliability of the above results, we conducted a simulation study in the context of the 2000–2002 cholera outbreak. Specifically, we used the generative model underlying our methodology (described above and in Methods) to generate a collection of synthetic outbreaks in order to

- investigate the impact on source estimation performance of changes in certain

fundamental implementation details; and

- compare the proposed method with a comparable established approach [12] (see Discussion).

We simulated $N = 851$ scenarios, where each node was allowed to be the epidemic source in turn. A given source node was infected at Day 1 and the first arrival-time of the epidemic at an arbitrary node is defined as the day on which the prevalence (i.e. the number of infected individuals) first exceeds 0.1% of the population. For each scenario, we then generated 400 realizations, 300 of which were used for training (i.e. estimating the spreading parameters and in turn calibrating the model) and the remaining 100 of which were used for testing, allowing us to compare the accuracy with which source estimates matched the true underlying sources.

We investigated the robustness in performance of our methodology, as a function of changing the number of observers, using different observer placement strategies, and incorporating prior knowledge or not. Specifically, we varied the

1. number of observers: 9 or 18 observers representing 1% or 2% of the total number of nodes, respectively.
2. observer placement strategies: random observer selection (random) or high-degree observer placement strategy (high-degree) [12], i.e. selecting observers with the highest (weighted) node degrees in the human mobility network.
3. incorporation of prior knowledge: informative prior, where the prior is proportional to each node's R_0 (R_0 prior), and non-informative prior, following a uniform distribution (uniform). Nodes with larger R_0 are easier to be infected, so it is reasonable to let the prior be proportional to these values.

Accuracy of our methodology was quantified using the following four criteria with respect to the true source s^* :

1. the probability that the 0.95 credible region contains s^* ;
2. the size of the 0.95 credible region;
3. the probability that s^* is ranked among the Top 10;
4. the mean distance between s^* and the estimated source \hat{s} .

We classified the nodes into different groups according to the magnitudes of their R_0 (divided into 6 categories $[0, 0.9)$, $[0.9, 1.8)$, $[1.8, 2.7)$, $[2.7, 3.6)$, $[3.6, 4.5)$, $[4.5, \infty)$) and their populations (on a log base 10 scale, divided into three categories), and made box plots for the above four criteria as a function of the various conditions. See Supplemental Figures 8, 9, and 10.

Based on our simulation results, we can conclude the following:

1. The high-degree observer placement strategy outperforms the random placement strategy.
2. The frequency with which the true source s^* is ranked in the Top 10 increases, and the mean distance between the true source and the estimation decreases, with increasing number of observers. At the same time, there is also a small decrease in the coverage probability of the 95% credible region and a much larger decrease in the size of the 95% credible region.

3. When using the high-degree placement of observers, the performance corresponding to 9 observers and that corresponding to 18 observers are comparable.
4. Use of a prior proportional to R_0 yields better results than a uniform prior when the source has large R_0 .
5. Using either prior (uniform prior or prior proportional to R_0), empirical coverage probabilities of the 0.95 credibility regions are good (> 0.7) for sources with not too small R_0 's (> 1.8) or moderate population ($\log_{10} > 3.5$).
6. It is possible for the 0.95 confidence sets to contain over 100 nodes. However, these sets will be substantially smaller (e.g., 10's of nodes) and have good coverage probabilities if the R_0 of the sources are not too small (> 1.8) and the population is large ($\log_{10} \geq 4.5$).
7. For the probability of the true source being in the Top 10 to be at least 0.5, under a uniform prior, the R_0 of sources should not be too small (> 1.8) and the population should be large (\log_{10} -base ≥ 4.5). Under a prior proportional to R_0 , the R_0 of sources should be larger (over 2.7).
8. Using either prior (uniform or proportional to R_0), if the true source has moderate R_0 (≥ 2.7) and large population ($\log_{10} \geq 4.5$), the distance between true and estimated sources can be smaller than 50 (km).

In general, as can be expected, our proposed method has good performance when the source node/city has moderate or large R_0 and population. These simulation results also suggest the following guidelines for usage of our methodology in practice:

1. To monitor spreads of epidemics, placing resources onto transportation hubs, i.e. 'high-degree' nodes is preferred.
2. There are 79.1% nodes having $R_0 > 1.8$ or moderate population ($\log_{10} > 3.5$). Thus although we will not know the R_0 and the population of the true source beforehand, there are still large chances we can ensure good (> 0.7) coverage probabilities.
3. There are only about 5% nodes with large population ($\log_{10} \geq 4.5$) thus the chance that we have small credible region (10's of nodes) with reasonable coverage is small. However, if we use 18 observers, in most cases we can ensure good coverage (as Item 5 in the conclusion list describes) with credible regions less than 100 nodes, which are usually feasible.
4. If we use a prior proportional to R_0 , there is a large chance that the probability of the true source being in the Top 10 to be at least 0.5, which is 41.5% (We only need the source has large(> 2.7) R_0), comparing with using the uniform prior case - where there is only less than 5% chance that the source fulfills the requirements described in Item 7 in the conclusion list.

Discussion

Tracking the source of an epidemic outbreak is of crucial importance in epidemiology. Indeed, the identification of the area or the human community that sparked an outbreak is useful not only for the short-term disease control, i.e. focusing interventions in the area in an effort to stop the transmission, but also for the long-term management of the

disease as such area could be the designated target of future interventions to curb the risk of new outbreaks. Therefore, the source detection problem is relevant not only in real-time, but also retrospectively on past data. However, the correct identification is often impaired by the lack of widespread and efficient surveillance networks, especially in developing countries. Even in the cases where such health infrastructures exist, the simple analysis of the data to identify the area where the first cases were reported might lead to an incorrect identification of the true source. In fact, the real beginning of an outbreak could go unreported because initial cases are misdiagnosed. This is the case for instance with cholera, for which lab confirmation of suspected cases is typically performed routinely only when an ongoing outbreak is declared. In this context, thus, mathematical models for source identification are of primary importance.

In this paper, we developed a framework that allows the probabilistic identification of the source based on first-arrival times of the infection on a small subset of nodes (e.g. human communities) used as observers, thus potentially reducing the cost to set up and maintain a surveillance network. From a mathematical perspective, we recast the source detection problem as identifying a relevant mixture component in a multivariate Gaussian mixture model. The framework is complemented by a stochastic spatially-explicit epidemiological model that embeds information about the human mobility network and is used to calibrate the parameters characterizing the probability distributions of first arrival-times. With our approach we address the major challenges stated by [5]. Building on the sensor-based Gaussian mixture approach, our data needs are realistic for practical settings. Additionally, the implementation is computationally feasible in large networks. Furthermore, we allow generic networks for the underlying spreading pattern (in contrast to assuming a tree-like structure). Moreover, adopting a Bayesian perspective opens the possibility to seamlessly integrate available nontrivial prior knowledge from previously observed spreading pattern or other data sources. While there are many methods for source detection, it is comparatively more rare that they also quantify the estimator accuracy, and none with an informed Bayesian prior probability distribution. Also note that our uncertainty quantification does not take into account uncertainty in the model components including gravity model and human mobility, epidemiological model for cholera spread, etc. These components are almost certainly idealized and only, at best, useful rather than correct. Thus practitioners should interpret the numbers coming at guiding decision making rather than absolute truths. We define (a) statistically well-defined region(s) of nodes that are likely to be the spreading origin of the observed process. Because this region need not be contiguous, it also arguably provides some information on the prospect for multiple sources (although we do not formally solve here the problem of detecting multiple sources, which is notably more complex).

Among existing methods in the literature, our method can perhaps be viewed as closest to the seminal work of Pinto *et al.* [12], which has been shown to be quite competitive with many other methods under a variety of scenarios [5]. However, for the specific context of water-borne diseases studied here, our method substantially outperforms that of Pinto *et al.* in simulation (see Fig 11, in Supplemental Materials). This advantage illustrates the value-added yielded by our use of highly informative prior information, i.e., through (i) utilization of the full human mobility network, (ii) encoding of prior information on quality of water and toilet facilities, and (iii) integration of a stochastic spatially-explicit epidemiological model to calibrate the means and covariances in our Gaussian mixtures.

The capability of the proposed method is demonstrated in the context of the 2000-2002 cholera outbreak in the KwaZulu-Natal province, through analyses of both actual data from the outbreak and a corresponding collection of synthetic experiments. In the experiments, we showed that the proposed method performs well if the source

has moderate or larger R_0 and population. Examination of experimental output suggests that the decay in performance in the case of small R_0 or population may be due to a lack of fit with the assumed multivariate Gaussian in the mixture model at the core of our framework. While simulation suggests that the Gaussian can be quite reasonable otherwise (see Fig 12 and Fig 13, in Supplemental Materials), the use of more general mixture models may help (e.g., nonparametric Bayesian mixtures [20]). However, it is not immediately apparent how best to integrate such models with an underlying epidemiological model. Alternatively, one might instead specify a mixture of epidemiological models, each defined conditional on a different node being the source. However, posterior-based inference of the source under this approach is likely to be nontrivial to implement, since even just parameter estimation in a single such version of our underlying epidemiological model has been found to require the use of sophisticated Markov chain Monte Carlo algorithms [21]. Accordingly, our proposed approach – detecting sources through posterior-based inference in Gaussian mixture models, with mean and covariance parameters informed by epidemiological models – may be viewed as a compromise that allows for increased interpretability and computational efficiency, arguably blending statistical and mathematical modeling in the spirit of data assimilation techniques.

We note that our analysis of the KwaZulu-Natal data is a retrospective study in nature - we effectively work from those nodes with sufficiently high prevalence and infer ‘backwards’ through the human mobility network to putative sources. Importantly, those nodes with insufficient prevalence do not contribute to the analysis (i.e., the difference in observer times with these nodes is right-censored and hence effectively infinity). A prospective study would potentially yield different results, depending on the choice of observer set. For example, if the observer set is chosen to contain the union of the two sets we have used in this paper (i.e., for Waves 1 and 2, respectively), then the results will be unchanged. On the other hand, to the extent that a common observer set contains only part or none of the two wave-specific sets we used, the results will change, and can be expected to degrade.

Finally, the framework and the results presented herein allow preliminary delineating a road-map to set up a surveillance network based on the proposed method in a country. The first step should consist in retrieving data on the spatial distribution of population. Available global sources are, e.g., WorldPop (www.worldpop.org), LandScan (landscan.ornl.gov) or the Global Human Settlement Layer (ghsl.jrc.ec.europa.eu). Then, possible census data on WASH (Water, Sanitation and Hygiene) conditions, e.g. access to tap water or toilet facilities, should be sought in order to possibly characterize the spatial heterogeneity of the Basic Reproductive number R_0 . Once such information is collected, the spatially-explicit stochastic epidemiological model can be set up. If data on past outbreaks are available, critical epidemiological parameters can be estimated using such information. Otherwise, reference literature values for such parameters can be assumed. As previously described, simulations of the epidemiological model are used to calibrate the parameters of the probability distributions of first-arrival times. An analysis as the one reported in section *Synthetic experiments* is also recommended to select the best strategy to allocate the observer nodes. Once the number and the location of the observer nodes are decided, an epidemiological surveillance system instructed to routinely perform lab testing for each suspect case of the selected disease is to be established. If an outbreak occurs, data on first arrival times at the selected nodes should readily allow the inference of the possible region of the source of the outbreak, thus enabling fast and effective interventions.

Methods

Gaussian source estimation with prior information

Following [12], we cast the source detection problem as identifying the relevant mixture component in a multivariate Gaussian mixture model. However, from the Bayesian perspective we adopt here, whereas the authors in [12] use a uniform prior over sources in their formulation, here we incorporate substantially more structured prior information. This structure arises both through the use of potentially nonuniform priors over sources (i.e., informed by local values of R_0) and through calibration of the multivariate Gaussian parameters using a human mobility network and a stochastic epidemiological model.

Let π_s be the prior probability of node $s \in V$ being the source and let \mathbf{t} be the K -dimensional vector of observed first-arrival times. Conditional on s being the true source, \mathbf{t} is assumed to follow a multivariate Gaussian distribution, with mean vector $\boldsymbol{\mu}_s$ and covariance matrix $\boldsymbol{\Lambda}_s$. Denote the corresponding density function by $\phi(\mathbf{t}; \boldsymbol{\mu}_s, \boldsymbol{\Lambda}_s)$. Then \mathbf{t} has density

$$\sum_{j=1}^N \pi_j \phi(\mathbf{t}; \boldsymbol{\mu}_j, \boldsymbol{\Lambda}_j). \quad (3)$$

A point estimate \hat{s} of the true source, say s^* , can be obtained by maximizing the posterior probability computed by Bayes theorem, i.e.

$$\hat{s} = \arg \max_{s \in V} P(S = s | \mathbf{t}) = \arg \max_{s \in V} \frac{\pi_s \phi(\mathbf{t}; \boldsymbol{\mu}_s, \boldsymbol{\Lambda}_s)}{\sum_{j=1}^N \pi_j \phi(\mathbf{t}; \boldsymbol{\mu}_j, \boldsymbol{\Lambda}_j)}.$$

The formula above can be written as:

$$\hat{s} = \arg \max_{s \in V} \left\{ -\frac{1}{2} (\mathbf{t} - \boldsymbol{\mu}_s)^\top \boldsymbol{\Lambda}_s^{-1} (\mathbf{t} - \boldsymbol{\mu}_s) + \log \pi_s \right\}. \quad (4)$$

Hence, this approach is equivalent to standard linear discriminant analysis for K -dimensional classification, with pre-defined class weights [33]. The Gaussian source estimator by [12] is a special case, assuming a uniform prior, i.e., $\pi_1 = \dots = \pi_K = 1/K$.

A set estimate \hat{C} for s^* may be obtained in the form of a highest posterior density (HPD) region, by applying the largest threshold τ_α corresponding to choice of a pre-specified α so that

$$\hat{C} = \{s : P(s | \mathbf{T} = \mathbf{t}) > \tau_\alpha\}, \text{ so that } \sum_{s \in \hat{C}} P(s | \mathbf{T} = \mathbf{t}) \geq 1 - \alpha. \quad (5)$$

The HPD region fulfills the condition that $P(s | \mathbf{T} = \mathbf{t}) > P(\tilde{s} | \mathbf{T} = \mathbf{t})$ for all $s \in \hat{C}$ and $\tilde{s} \notin \hat{C}$, and consequently minimizes the volume of the area covered, among all sets with at least $1 - \alpha$ posterior mass [34]. Note that this definition does not consider distance with respect to the network connectivity. Furthermore the HPD region does not necessarily need to be a connected subgraph of the network.

Parameter calibration using a human mobility network and the stochastic epidemiological model

In order to produce the point and/or set estimates \hat{s} and \hat{C} , values must be available for the mean and covariance parameters $\boldsymbol{\mu}_s$ and $\boldsymbol{\Lambda}_s$ of each Gaussian component. There are deterministic estimates available for these parameters, which can be derived easily from network topology information only, using shortest path lengths between potential source

candidates and sensors [12]. But μ_s and Λ_s – representing first and second order information on the behavior of the first arrival times \mathbf{t} – are reflective of what in the current setting is typically a highly complex stochastic phenomenon. Accordingly, we instead calibrate these values in our model using a stochastic epidemiological model that integrates human mobility network information.

A stochastic, spatially-explicit epidemiological model for the transmission of cholera, a prototypical waterborne disease, has been introduced in [23]. This model considers a set of human communities interconnected by a mobility network and describes the temporal evolution of the integer number of susceptible (\mathcal{S}_i), infected (\mathcal{I}_i), and recovered (\mathcal{R}_i) individuals hosted in the nodes i of the network. Additionally, the model incorporates the evolution of the environmental concentration of bacteria (\mathcal{B}_i). Specifically, all events involving human individuals (births, deaths and changes of epidemiological status) are treated as stochastic events that occur at rates that depend on the state of the system. The possible events and their corresponding rates are shown in Table 1.

Table 1. Transitions and rates of occurrence of all possible events in a node i .

Event	Transition	Rate
Birth	$(\mathcal{S}_i, \mathcal{I}_i, \mathcal{R}_i) \rightarrow (\mathcal{S}_i + 1, \mathcal{I}_i, \mathcal{R}_i)$	$\nu_i^1 = \mu H_i$
Death of a susceptible	$(\mathcal{S}_i, \mathcal{I}_i, \mathcal{R}_i) \rightarrow (\mathcal{S}_i - 1, \mathcal{I}_i, \mathcal{R}_i)$	$\nu_i^2 = \mu \mathcal{S}_i$
Symptomatic infection	$(\mathcal{S}_i, \mathcal{I}_i, \mathcal{R}_i) \rightarrow (\mathcal{S}_i - 1, \mathcal{I}_i + 1, \mathcal{R}_i)$	$\nu_i^3 = \sigma \mathcal{F}_i \mathcal{S}_i$
Death of an infected	$(\mathcal{S}_i, \mathcal{I}_i, \mathcal{R}_i) \rightarrow (\mathcal{S}_i, \mathcal{I}_i - 1, \mathcal{R}_i)$	$\nu_i^4 = \mu \mathcal{I}_i$
Cholera-induced death	$(\mathcal{S}_i, \mathcal{I}_i, \mathcal{R}_i) \rightarrow (\mathcal{S}_i, \mathcal{I}_i - 1, \mathcal{R}_i)$	$\nu_i^5 = \alpha \mathcal{I}_i$
Recovery of an infected	$(\mathcal{S}_i, \mathcal{I}_i, \mathcal{R}_i) \rightarrow (\mathcal{S}_i, \mathcal{I}_i - 1, \mathcal{R}_i + 1)$	$\nu_i^6 = \gamma \mathcal{I}_i$
Asymptomatic infection	$(\mathcal{S}_i, \mathcal{I}_i, \mathcal{R}_i) \rightarrow (\mathcal{S}_i - 1, \mathcal{I}_i, \mathcal{R}_i + 1)$	$\nu_i^7 = (1 - \sigma) \mathcal{F}_i \mathcal{S}_i$
Death of a recovered	$(\mathcal{S}_i, \mathcal{I}_i, \mathcal{R}_i) \rightarrow (\mathcal{S}_i, \mathcal{I}_i, \mathcal{R}_i - 1)$	$\nu_i^8 = \mu \mathcal{R}_i$
Immunity loss	$(\mathcal{S}_i, \mathcal{I}_i, \mathcal{R}_i) \rightarrow (\mathcal{S}_i + 1, \mathcal{I}_i, \mathcal{R}_i - 1)$	$\nu_i^9 = \rho \mathcal{R}_i$

Table 1 shows transitions and rates of occurrence for all possible events indexed by a given node i . The generic event k occurs in node i at rate ν_i^k . The population of each node is assumed to be at demographic equilibrium, with μ being the human mortality rate and μH_i a constant recruitment rate. The force of infection, which represents the rate at which susceptible individuals become infected due to contact with contaminated water, is defined as:

$$\mathcal{F}_i = \beta_i \left[(1 - m) \frac{\mathcal{B}_i}{K + \mathcal{B}_i} + m \sum_{j=1}^n Q_{ij} \frac{\mathcal{B}_j}{K + \mathcal{B}_j} \right].$$

The parameter β_i represents the exposure rate. The fraction $\mathcal{B}_i/(K + \mathcal{B}_i)$ is the probability of becoming infected due to the exposure to a concentration \mathcal{B}_i of *V. cholerae*, K being the half-saturation constant [35]. Because of human mobility, a susceptible individual residing at node i can be exposed to pathogens in the destination community j . This is modeled assuming that the force of infection in a given node depends on the local concentration \mathcal{B}_i for a fraction $(1 - m)$ of the susceptible hosts and on the concentration \mathcal{B}_j of the surrounding communities for the remaining fraction m . The parameter m thus represents the community-level probability that individuals travel outside their node and is assumed, in this formulation, to be node-independent. The concentrations \mathcal{B}_j are weighted according to the probabilities Q_{ij} that an individual living in node i would reach j as a destination. Matrix Q thus epitomizes information about human mobility. Formally, human mobility patterns are defined

according to a gravity model in this approach. Q_{ij} is defined as:

$$Q_{ij} = \frac{H_j e^{-d_{ij}/D}}{\sum_{k \neq i}^n H_k e^{-d_{ik}/D}},$$

where the attractiveness factor of node j depends on its population size, while the deterrence factor is assumed to be dependent on the distance d_{ij} between the two communities and represented by an exponential kernel (with shape factor D).

Concentration $\mathcal{B}_i(t)$ is modeled as a stochastic variable in continuous time, as the number of bacteria is expected to be large enough to allow a continuous representation. Its evolution is described by:

$$\frac{d\mathcal{B}_i}{dt} = -\mu_B \mathcal{B}_i + \frac{p_i}{W_i} \mathcal{I}_i,$$

where μ_B is the mortality rate of the bacteria in the environment, p_i is the rate at which bacteria produced by one infected person reach and contaminate the local water reservoir of volume W_i , and \mathcal{I}_i is the number of infected.

Assuming a single node s as the source of the epidemic, the stochastic model just described allows for the generation of multiple Monte Carlo realizations of the outbreak. From these realizations we may obtain estimates of the mean and covariance parameters $\boldsymbol{\mu}_s$ and $\boldsymbol{\Lambda}_s$ for the first-arrival times \mathbf{t} at the observers. (Methods of numerical integration or similar might be used here instead.) This procedure is repeated assuming each node in turn as a potential source. To estimate $\boldsymbol{\mu}_s$ accurately we rely on large-sample properties of simple averaging. However, our estimation of $\boldsymbol{\Lambda}_s$ was found to benefit from the use of shrinkage methods. We adopted the approach of [36], which assumes zero covariance among off-diagonal elements (supported by our data, most likely due to the sparse and distributed nature of our observer nodes), but heterogeneous variances, which are estimated using a distribution-free shrinkage towards the median.

Additional implementation details may be found in the Supplemental Text (S1 File). In particular, information on how we set the various rate parameters in our stochastic model may be found therein, with corresponding pointers to the supporting literature.

Supporting information

S1 Fig. Time course of initial epidemic spread: Wave 1.

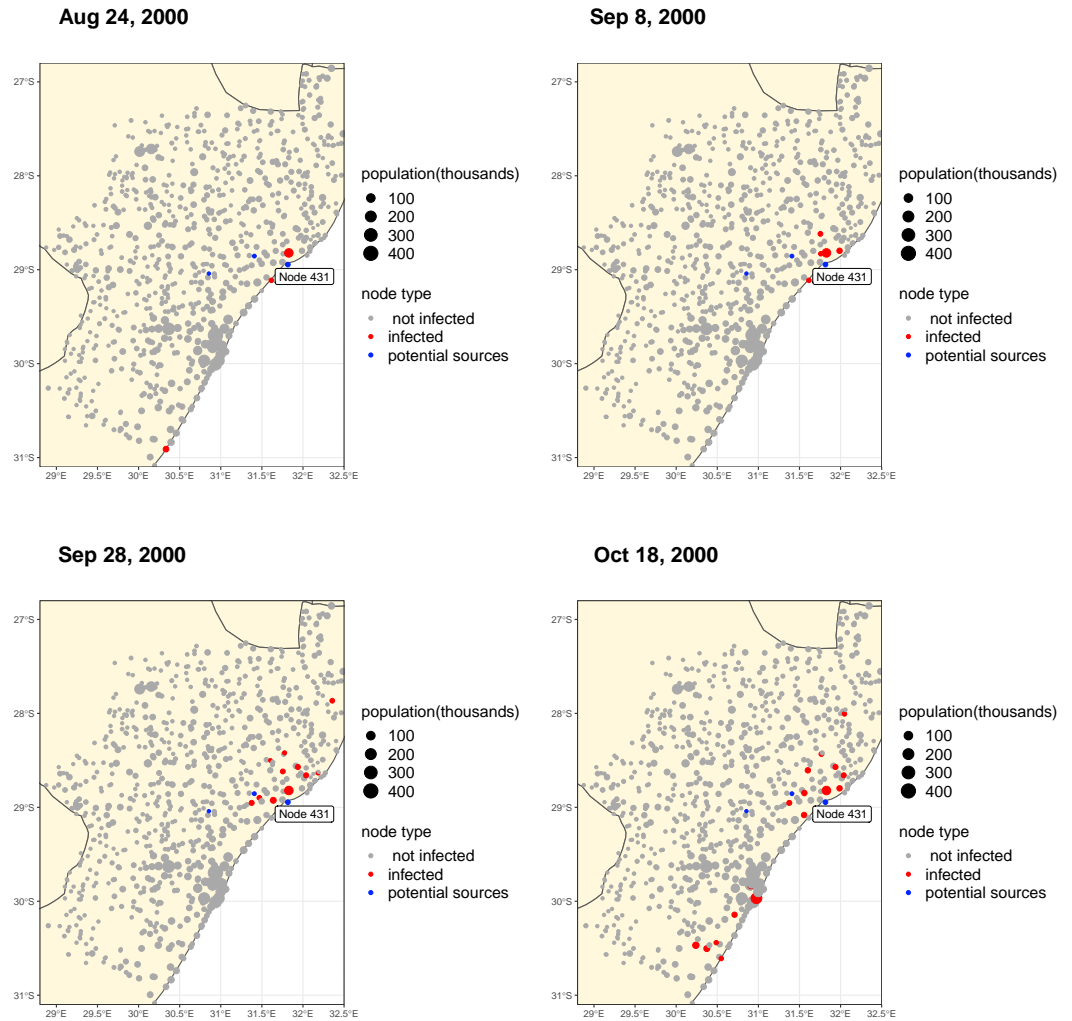


Fig 6. the 2000-2002 Cholera Outbreak, the first wave (Node 431: uMhlathuze Local Municipality, South Africa, 143km north to Durban)

S2 Fig. Time course of initial epidemic spread: Wave 2.

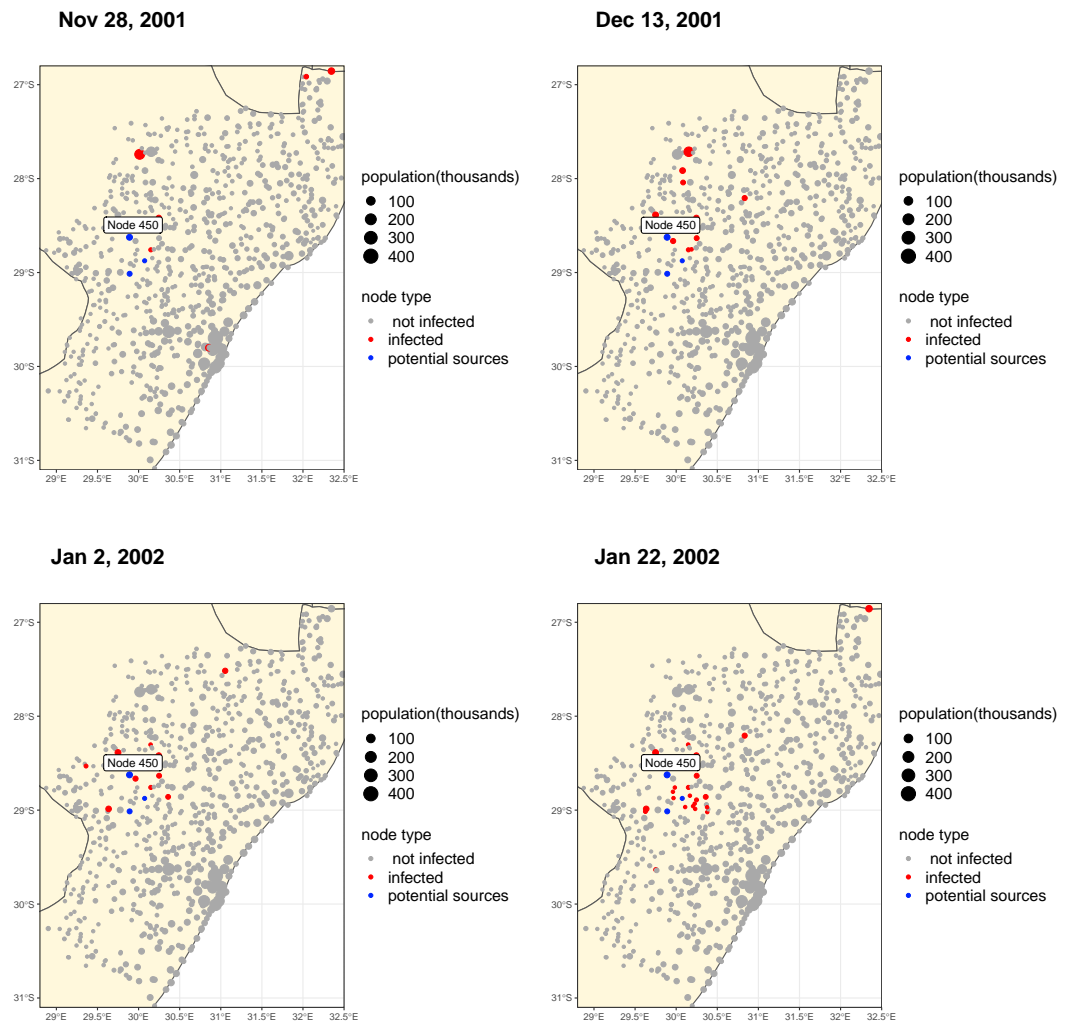


Fig 7. the 2000-2002 Cholera Outbreak, the second wave (Node 450: South west of town Ezakheni A, no far (17km) from Ladysmith to the south east)

S3 Fig.

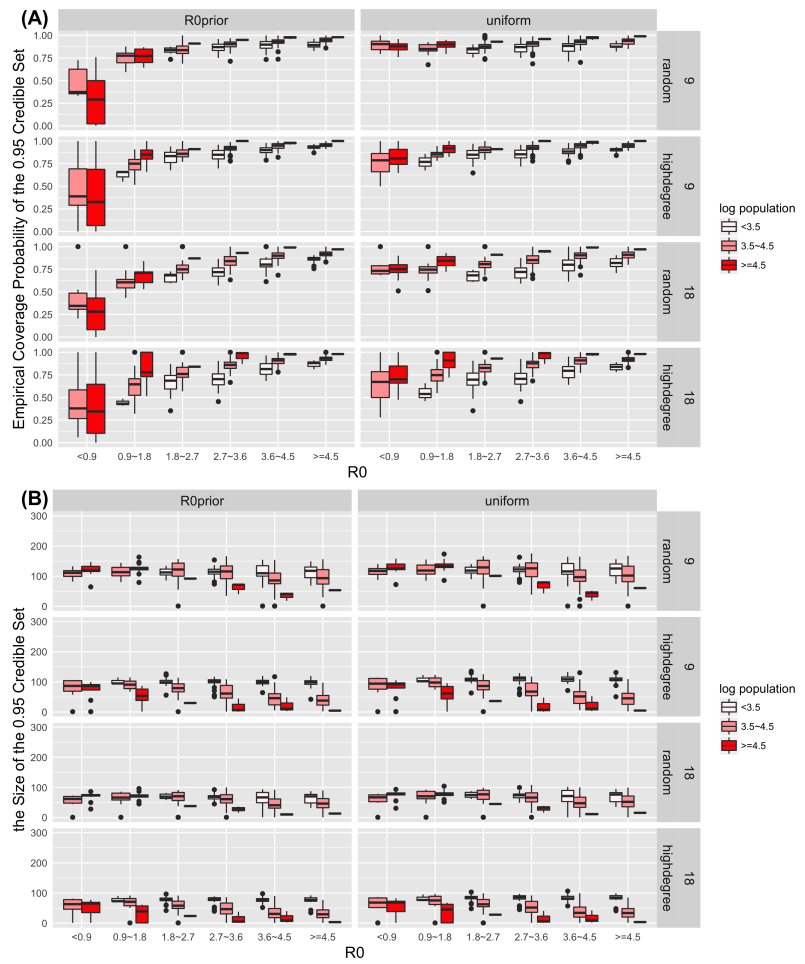


Fig 8. The Performance of the Proposed Method:(A) empirical coverage probability of the 95% credibility region and (B) the size of the 95% credibility region. Different simulation setting are shown: 9 or 18 observers, random and high-degree observer placement, and incorporation of informative R_0 prior and non-informative uniform prior knowledge.

S4 Fig.

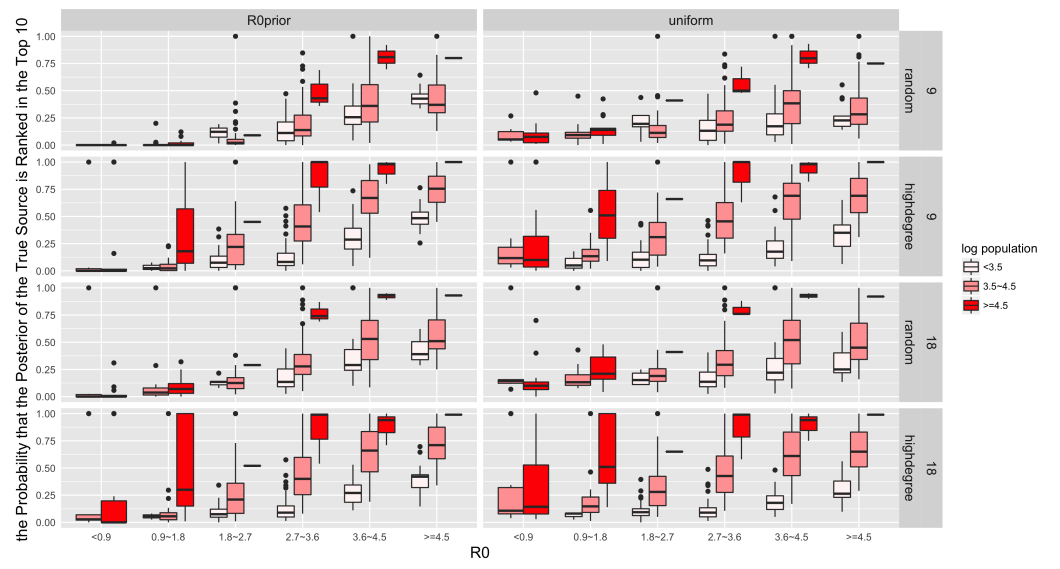


Fig 9. The Performance of the Proposed Method: The probability that the posterior of the true Source is ranked in the Top 10

S5 Fig.

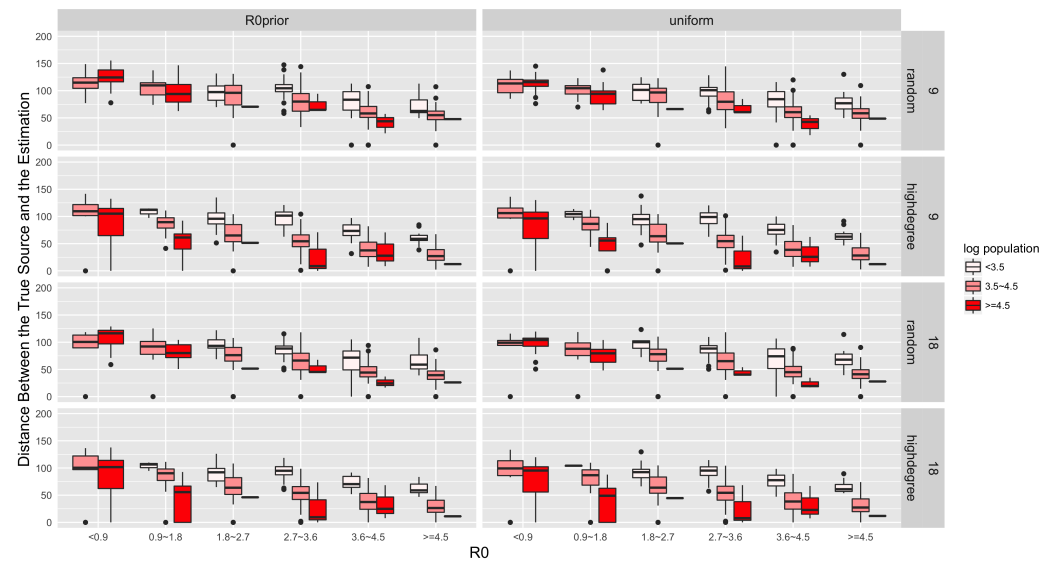


Fig 10. The Performance of the Proposed Method, Distance Between the True Source and the Estimation

S6 Fig.

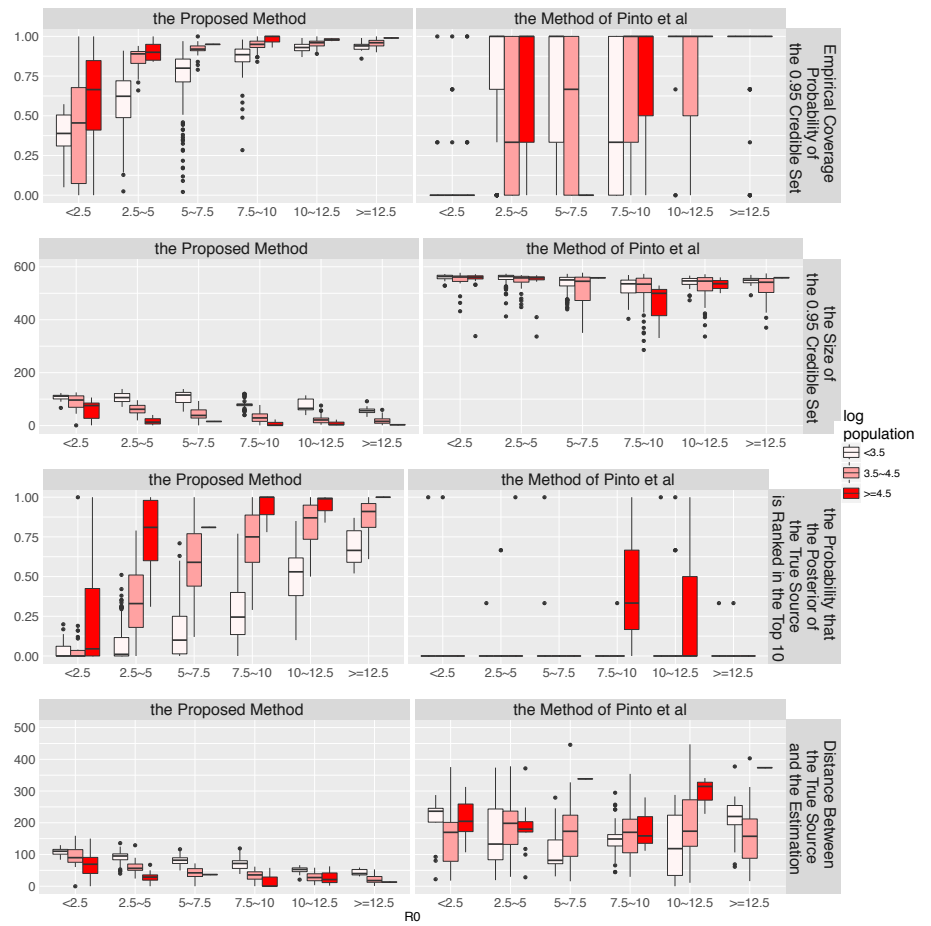


Fig 11. Comparison between the Proposed Method and Pinto's Method

S7 Fig.

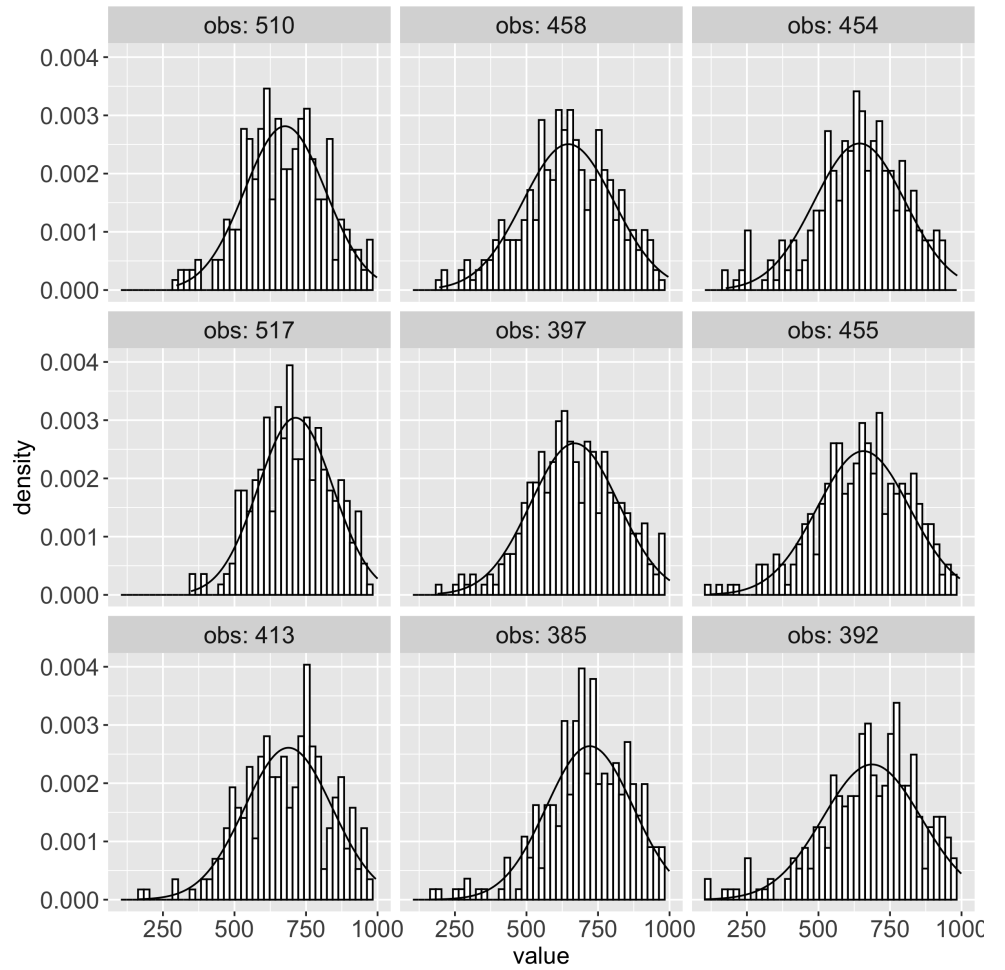


Fig 12. Visualizations illustrate that the quality of the Gaussian approximation is quite reasonable, under model assumptions. To illustrate, we used the 1st-ranked inferred source in the second wave as a source and simulated outcomes according to our model. The marginal distributions for arrival times at the various 2nd wave observers are shown above. We can see that a normal approximation agrees well with the histograms of arrival times.

S8 Fig.

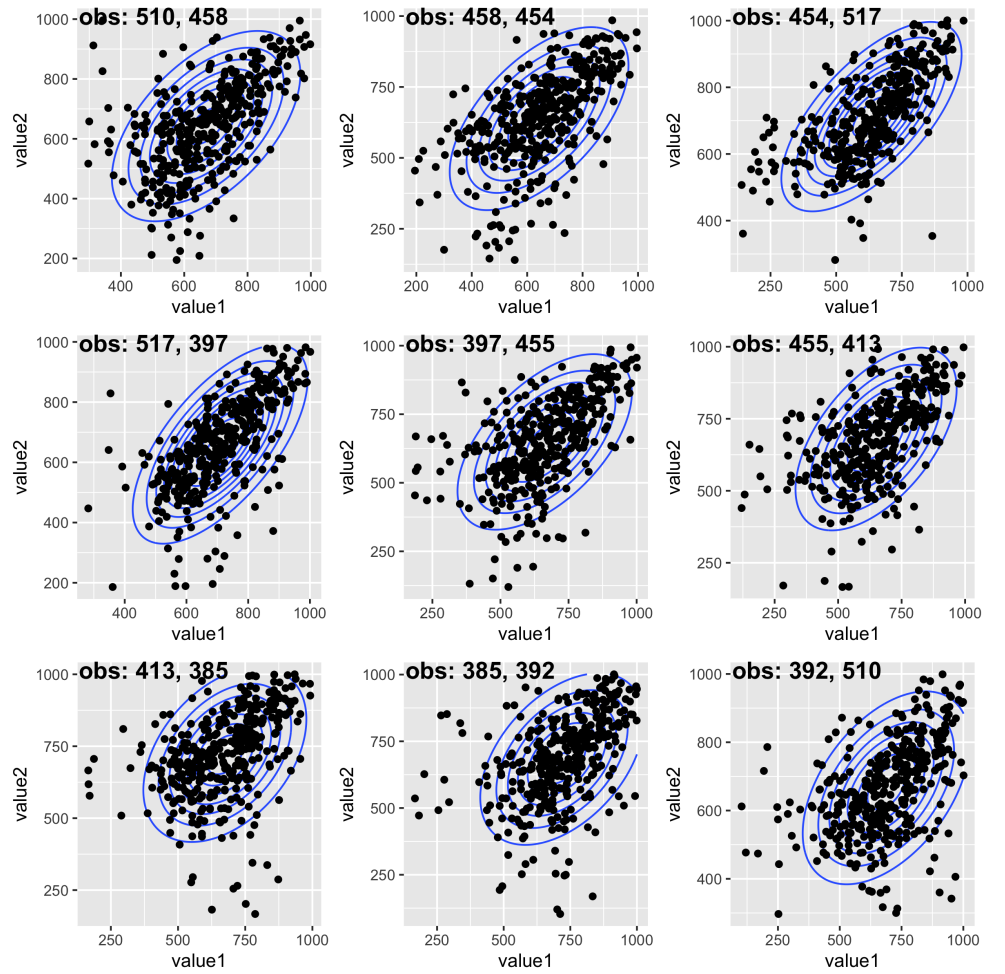


Fig 13. Bivariate plots tell a similar story for distributions across pairs of observer nodes, in that the bivariate scatterplots agree with the contour of normal distributions with same mean and covariance structure.

S9 Fig.

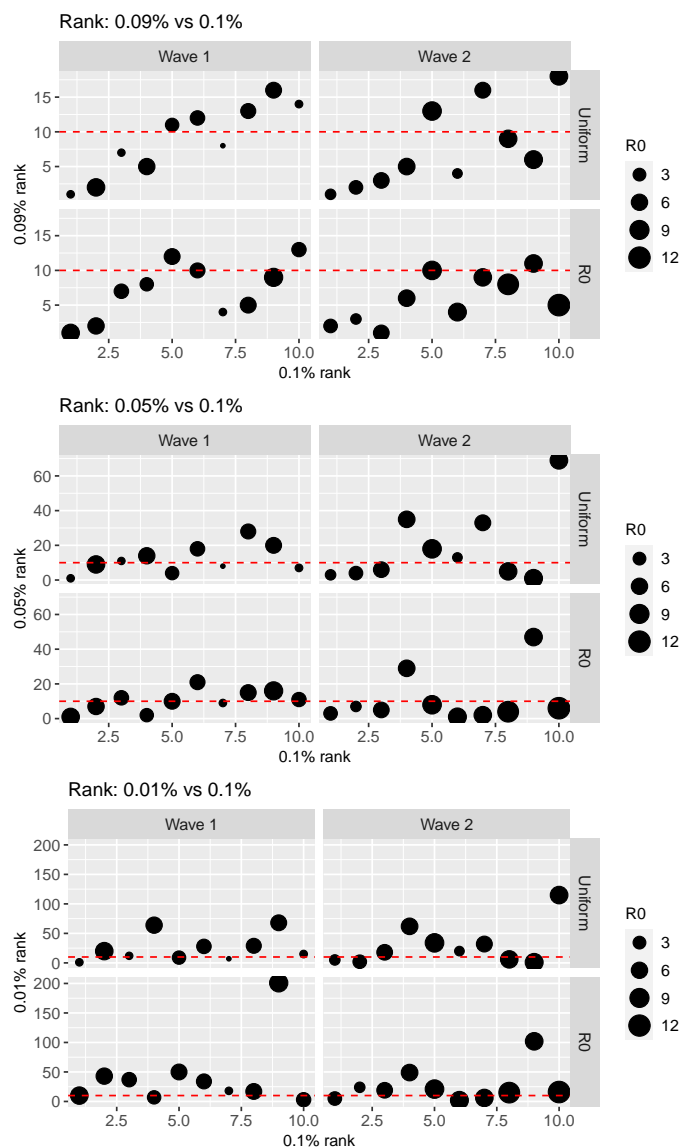


Fig 14. Sensitivity analysis shows that our results (i.e., the top-ten ranked nodes) remain robust when this choice of threshold is decreased to 0.09% and even 0.05%, but deteriorates at 0.01%.

S1 File. Additional details.

Small-world analysis of human mobility network

To interrogate the human mobility network for the small-world property, we implemented a variation on the analysis described in [37, Ch5.5.2], as adapted for weighted networks in [38]. Specifically, this consists of (i) calculating the average shortest path length and the (weighted) clustering coefficient for the human mobility networks, and (ii) comparing the resulting values to their distributions under an analogous random graph ensemble model. Here the random graph ensemble was defined through permutation of the weights in the original human mobility network (a fully connected, weighted network). Shortest path length was calculated based on a distance between nodes defined as the inverse of the corresponding weight on the respective link between those nodes. We find that whereas the average shortest path length in the original network (70.67) is on par with typical values in the random ensemble (minimum of 72.74, maximum of 73.36), its clustering coefficient (0.135) is orders of magnitude larger than the typical values in the random ensemble (minimum of 0.00241, maximum 0.00246). In other words, while the original network seems to share small shortest-path distances with a random graph, it exhibits substantially more clustering. Together, these two aspects suggest (weighted) small-world behavior.

Implementation details

We adopted the stochastic model of cholera transmission proposed in [23] focusing on the human mobility network and discarding the river network component. For the application to KwaZulu-Natal, we use the domain discretization and the demographic information from [21].

Following [23], we introduce for each node i the contamination rate θ_i that embeds information regarding the parameters p_i , K and W_i . We modulate the exposure, β_i , and contamination, θ_i , rates using census information on access to safe water and toilet facilities, respectively, as in [21]. Specifically: $\beta_i = \beta_{max} \cdot no\ water\ access\ rate$ and $\theta_i = \theta_{max} \cdot no\ toilet\ access\ rate$. Then R_0 for each node is calculated by:

$$R_0 = \frac{\theta\beta\sigma}{\mu_B(\gamma + \alpha + \mu)}$$

Table 2 summarizes the model parameters along with the literature references or notes for the assumed values.

Finally we set θ_{max} , which in turn controls the distribution of R_0 , so as to obtain an overall cholera incidence and time to epidemic peak comparable to the one observed. This resulted in $\theta_{max}=15\ day^{-1}$.

We used the model set up described above to simulate epidemic waves for a given source. We assume 0.1% population is symptomatic infected in the source node, i.e., $\mathcal{I}_i(t=0) = H_i \cdot 0.001$, where i is the index of the source and H_i is the population of that node. We could further calculate initial recovered population based on symptomatic ration σ : $\mathcal{R}_i(t=0) = (1 - \sigma)/\sigma \cdot \mathcal{I}_i(t=0)$. For all other nodes we set $\mathcal{S}_i(t=0) = H_i$, $\mathcal{I}_i(t=0) = \mathcal{R}_i(t=0) = \mathcal{B}_i(t=0) = 0$.

For each simulated realization, we look at 100-day time range at $\Delta t = 0.1$ day resolution. The number of susceptible, infected, recovered and corresponding cumulative cases are continuously updated according to the events in Table 1. Bacteria concentration vector \mathcal{B} is instead updated at every Δt solving analytically equation in Page 16 assuming a constant bacterial input (i.e. constant number of infected people) for the duration of the timestep. At each time point, we track the following 5 quantities:

Table 2. Model parameters

Parameters	Value	Explanation	Reference/Note
μ	$4.2 \cdot 10^{-5}$	population natality and mortality rate (1/day)	[21]
γ	0.2	rate at which people recover from cholera (1/day)	[23]
α	0	cholera induced mortality rate (1/day)	Cholera mortality is much lower than the recovery rate and thus can safely be neglected for what concerns the dynamics of the outbreak
σ	0.05	symptomatic ratio: fraction of infected people that develop symptoms and are infective	[21, 23]
μ_B	0.2	death rate of <i>V.cholerae</i> in the aquatic environment (1/day)	[21, 23]
ρ	0	immunity loss rate (1/day)	As disease induced immunity is believed to last some years, it can be neglected when studying the initial phase of an outbreak
β_{max}	1	maximum exposure rate (1/day)	[21]
D	50	distance scaling parameter (km)	[23]
m	0.3	the probability individuals leave their original nodes	[23]

susceptible, infected, recovered, bacteria concentration and cumulative cases at each node.

In this way, we tracked the number of the infected in each node in 100 days. Thus, for a particular source i and a set of observers, we got the observer infected dates for each realization. As we mentioned in synthetic experiments section, we generated 400 realizations, 300 of which were used for training, i.e., the 300 observer infected dates vectors are used to estimate mean vector μ_s and covariance matrix Λ_s in Methods - Gaussian source estimation with prior information section. Using either uniform prior or prior proportional to R_0 , we could get source estimations for the remaining 100 realizations, or estimations for real application waves.

The realizations simulation is the most computationally intensive part. We conducted parallel computing using Boston University Shared Computing Clusters. For each single job, we generated 5 realizations for a single node. The total simulation procedure took about 10 hours.

More insights on 2000–2002 South African cholera outbreak

Looking at the first wave observers, the observers are (from highest degree to lowest degree):

1. Node 604 - at Ntanyandlovu, 60km east to the coal mining town Dundee, on Regional Routes R68
2. Node 366 - at Mandeni, on Regional Routes R102
3. Node 519 - at Kliprivier, on Regional Routes R33
4. Node 707 - at Suburb of coal mining and cattle ranching town Vryheid, on Regional Routes R34
5. Node 465 - at Salofu, at a intersection of three unnamed roads
6. Node 451 - Near City Ladysmith by Tugela River
7. Node 408 - at Pholela, by Tugela River
8. Node 544 - at Phambana, at intersection of Old Tshokwane Rd and Road S129
9. Node 274 - at Mgwadumane, at the intersection of Hlimbitwa and Umvoti Rivers

We can see most of the first wave observers are on the Regional Routes and the others are by rivers. For the second wave ones:

1. Node 510 - at Watersmeet, by Kliprivier River
2. Node 458 - at Ngqulu, by Buffelsrivier River
3. Node 454 - at Bhaza, at the intersection of Sondagsrivier, Nhlanyanga, Munywana Rivers
4. Node 517 - at Waaihoek, at the intersection of Kalkoenspruit and Wasbankrivier River
5. Node 397 - at Gujini
6. Node 455 - at Mashunka, at the intersection of Sundays River and Tugela River
7. Node 413 - at Ezilozini, by Tugela River
8. Node 385 - at Estcourt
9. Node 392 - at Tugela Estates, at the intersection of Tugela River and its branches

Acknowledgments

Special thanks go to the KwaZuluNatal Department of Health for providing the data set that made this work possible. JL and EDK were supported in part by awards from the US Air Force Office of Scientific Research (12RSL042) and Army Research Office (W911NF-15-1-0440). JM was supported in part by the Alexander von Humboldt Foundation as well as the German Federal Ministry for Education and Research.

References

1. Zwingle E. Cities: Challenges for Humanity. *National Geographic*. 2002;22.
2. Fraser C, Donnelly CA, Cauchemez S, Hanage WP, Van Kerkhove MD, Hollingsworth TD, et al. Pandemic potential of a strain of influenza A (H1N1): early findings. *science*. 2009;324(5934):1557–1561.
3. Yusim K, Peeters M, Pybus OG, Bhattacharya T, Delaporte E, Mulanga C, et al. Using human immunodeficiency virus type 1 sequences to infer historical features of the acquired immune deficiency syndrome epidemic and human immunodeficiency virus evolution. *Philosophical Transactions of the Royal Society B: Biological Sciences*. 2001;356(1410):855–866.
4. Paraskevis D, Magiorkinis E, Magiorkinis G, Sypsa V, Papanicolaou V, Lazanas M, et al. Increasing prevalence of HIV-1 subtype A in Greece: estimating epidemic history and origin. *The Journal of infectious diseases*. 2007;196(8):1167–1176.
5. Jiang J, Wen S, Yu S, Xiang Y, Zhou W. Identifying propagation sources in networks: State-of-the-art and comparative studies. *IEEE Communications Surveys & Tutorials*. 2017;19(1):465–481.
6. Shah D, Zaman T. Detecting sources of computer viruses in networks: theory and experiment. In: *Proceedings of the ACM SIGMETRICS International Conference on Measurement and Modeling of Computer Systems*. ACM; 2010. p. 203–214.
7. Shah D, Zaman T. Rumor centrality: A Universal Source Detector. In: *Proceedings of the ACM SIGMETRICS International Conference on Measurement and Modeling of Computer Systems*. ACM; 2012. p. 199–210.
8. Zhu K, Ying L. Information source detection in the SIR model: A sample-path-based approach. *IEEE/ACM Transactions on Networking (TON)*. 2016;24(1):408–421.
9. Luo W, Tay WP, Leng M. On the universality of Jordan centers for estimating infection sources in tree networks. *IEEE Transactions on Information Theory*. 2017;63(7):4634–4657.
10. Brockmann D, Helbing D. The Hidden Geometry of Complex, Network-Driven Contagion Phenomena. *Science*. 2013;342(6164):1337–1342. doi:10.1126/science.1245200.
11. Manitz J, Harbering J, Schmidt M, Kneib T, Schöbel A. Source Estimation for Propagation Processes on Complex Networks with an Application to Delays in Public Transportation Systems. Accepted at JRSS-C. 2016;.
12. Pinto PC, Thiran P, Vetterli M. Locating the source of diffusion in large-scale networks. *Physical review letters*. 2012;109(6):068702.
13. Louni A, Subbalakshmi K. A two-stage algorithm to estimate the source of information diffusion in social media networks. In: *Computer Communications Workshops (INFOCOM WKSHPS), 2014 IEEE Conference on*. IEEE; 2014. p. 329–333.
14. Agaskar A, Lu YM. A fast monte carlo algorithm for source localization on graphs. In: *Wavelets and Sparsity XV*. vol. 8858. International Society for Optics and Photonics; 2013. p. 88581N.

15. Colizza V, Barrat A, Barthélemy M, Vespignani A. The role of the airline transportation network in the prediction and predictability of global epidemics. *Proceedings of the National Academy of Sciences*. 2006;103(7):2015–2020. doi:10.1073/pnas.0510525103.
16. Balcan D, Colizza V, Gonçalves B, Hu H, Ramasco JJ, Vespignani A. Multiscale mobility networks and the spatial spreading of infectious diseases. *Proceedings of the National Academy of Sciences*. 2009;106(51):21484–21489. doi:10.1073/pnas.0906910106.
17. Meloni S, Perra N, Arenas A, Gómez S, Moreno Y, Vespignani A. Modeling human mobility responses to the large-scale spreading of infectious diseases. *Scientific reports*. 2011;1:62.
18. Bajardi P, Poletto C, Ramasco JJ, Tizzoni M, Colizza V, Vespignani A. Human mobility networks, travel restrictions, and the global spread of 2009 H1N1 pandemic. *PloS one*. 2011;6(1):e16591.
19. Chao DL, Halloran ME, Longini IM. Vaccination strategies for epidemic cholera in Haiti with implications for the developing world. *Proceedings of the National Academy of Sciences*. 2011;108(17):7081–7085.
20. Gershman SJ, Blei DM. A tutorial on Bayesian nonparametric models. *Journal of Mathematical Psychology*. 2012;56(1):1–12.
21. Mari L, Bertuzzo E, Righetto L, Casagrandi R, Gatto M, Rodriguez-Iturbe I, et al. Modelling cholera epidemics: the role of waterways, human mobility and sanitation. *Journal of the Royal Society Interface*. 2012;9(67):376–388.
22. Rinaldo A, Bertuzzo E, Mari L, Righetto L, Blokesch M, Gatto M, et al. Reassessment of the 2010-2011 Haiti cholera outbreak and rainfall-driven multiseason projections. *Proceedings of the National Academy of Sciences of the United States of America*. 2012;109(17):6602–6607.
23. Bertuzzo E, Finger F, Mari L, Gatto M, Rinaldo A. On the probability of extinction of the Haiti cholera epidemic. *Stochastic Environmental Research and Risk Assessment*. 2016;30(8):2043–2055.
24. Altarelli F, Braunstein A, Dall’Asta L, Lage-Castellanos A, Zecchina R. <https://www.overleaf.com/project/5c8aaaba668c4d484dda1716> Bayesian inference of epidemics on networks via belief propagation. *Physical review letters*. 2014;112(11), 118701.
25. Lokhov AY, Mézard M, Ohta H, Zdeborová L. Inferring the origin of an epidemic with a dynamic message-passing algorithm. *Physical Review E*, 2014;90(1), 012801.
26. Antulov-Fantulin N, Lančić A, Šmuc T, Štefančić H, Šikić M. Identification of patient zero in static and temporal networks: Robustness and limitations. *Physical review letters*. 2015;114(24), 248701.
27. Manitz J, Kneib T, Schlather M, Helbing D, Brockmann D. Origin detection during food-borne disease outbreaks—a case study of the 2011 ehec/hus outbreak in Germany. *PLoS currents*. 2014;6.
28. Horn AL, Friedrich H. Locating the source of large-scale outbreaks of foodborne disease. *Journal of the Royal Society Interface*. 2019;16(151), 20180624.

29. Agaskar A, Lu YM. A fast monte carlo algorithm for source localization on graphs. In *Wavelets and Sparsity XV* (Vol. 8858, p. 88581N). International Society for Optics and Photonics. 2013.
30. Bertuzzo E, Azaele S, Maritan A, Gatto M, Rodriguez-Iturbe I, Rinaldo A. On the space-time evolution of a cholera epidemic. *Water Resources Research*. 2008;44(1).
31. Gatto M, Mari L, Bertuzzo E, Casagrandi R, Righetto L, Rodriguez-Iturbe I, et al. Generalized reproduction numbers and the prediction of patterns in waterborne disease. *Proceedings of the National Academy of Sciences USA*. 2012;48:19703–19708.
32. Gatto M, Mari L, Bertuzzo E, Casagrandi R, Righetto L, Rodriguez-Iturbe I, et al. Spatially explicit conditions for waterborne pathogen invasion. *The American Naturalist*. 2013;182:328–346.
33. Anderson TW. *An Introduction to Multivariate Statistical Analysis*. Wiley Series in Probability and Statistics. Wiley; 2003. Available from: <https://books.google.com.ng/books?id=Cmm9QgAACAAJ>.
34. Casella G, Berger RL. *Statistical inference*. vol. 2. Duxbury Pacific Grove, CA; 2002.
35. Codeço C. Endemic and epidemic dynamics of cholera: the role of the aquatic reservoir. *BMC Infectious Diseases*. 2001;1(1).
36. Opgen-Rhein R, Strimmer K. Accurate ranking of differentially expressed genes by a distribution-free shrinkage approach. *Statistical applications in genetics and molecular biology*. 2007;6(1).
37. Kolaczyk ED, Csárdi G. *Statistical analysis of network data with R* (Vol. 65). New York, NY: Springer. 2014.
38. Li W., Lin Y., Liu, Y. (2007). The structure of weighted small-world networks. *Physica A: Statistical Mechanics and its Applications*. 2007; 376, 708-718.